

The effect of spatial scales on the reproductive fitness of plant pathogens

Alexey Mikaberidze^{*,1},
Christopher C. Mundt²,
Sebastian Bonhoeffer¹

*alexey.mikaberidze@env.ethz.ch, Institute of Integrative Biology, ETH Zurich, CHN H 75.1, Universitaetstrasse 16, 8092, Zurich, phone: +41 44 632 26 02

¹Institute of Integrative Biology, ETH Zurich

²Department of Botany and Plant Pathology, Oregon State University

Keywords: basic reproductive number disease control disease gradient dispersal epidemiology host-pathogen interaction mathematical model plant disease population dynamics spatial scales

Abstract

Plant diseases often cause serious yield losses in agriculture. A pathogen's reproductive fitness can be quantified by the basic reproductive number, R_0 . Since pathogen transmission between host plants depends on the spatial separation between them, R_0 is strongly influenced by the spatial scales of pathogen dispersal and the spatial scales of the host population.

We propose a novel method to estimate the basic reproductive number as a function of the size of a field planted with crops and its aspect ratio. This approach is based on measurements of disease gradients and uses a spatially explicit population dynamical model.

The basic reproductive number was found to increase with the field size at small field sizes and to saturate to a constant value at large field sizes. It reaches a maximum in square fields and decreases as the field becomes elongated. This pattern appears to be quite general: it holds for dispersal kernels that decrease exponentially or faster as well as for fat-tailed dispersal kernels that decrease slower than exponential (i.e. power-law kernels).

We used this approach to estimate R_0 in wheat stripe rust (an important disease caused by *Puccinia striiformis*), since disease gradients for this pathogen were thoroughly measured over large distances [Sackett and Mundt, *Phytopathology*, 95, 983 (2005)]. For the two largest datasets, we estimated R_0 in the limit of large fields to be of the order of 50. These estimates are consistent with independent field observations [Cowger et al. (2005), *Phytopathology*, 95, 97282; Farber et al. (2013), *Phytopathology*, 103, 41].

We present a proof of principle of a novel approach to estimate the basic reproductive number, R_0 , of plant pathogens using wheat stripe rust as a case study. We found that the spatial extent over which R_0 changes strongly is quite fine-scaled (about 30 m of the linear extension of the field). Our results indicate that in order to optimize the spatial scale of deployment of fungicides or host resistances, the adjustments should be made at a fine spatial scale.

1. Introduction

When plant pathogens succeed in infecting their hosts, they colonize the host tissue and deprive hosts of resources and energy. This often leads to serious yield losses in agriculture (Strange and Scott, 2005). Disease-resistant crop varieties and chemicals (fungicides or antibiotics) are widely used to control infectious diseases of plants. But both of these control measures are highly vulnerable to pathogen adaptation: pathogens evolve to overcome host resistances and to become insensitive to fungicides (McDonald and Linde, 2002). In order to devise effective and durable strategies of disease control (Mundt, 2014), a thorough understanding of basic epidemiological properties of plant pathogens with the help of appropriate mathematical models is necessary.

The spread of infectious diseases depends on the contact structure, a network in which each host is a node and has a number of weighted, directional links to other hosts. The strength of each link represents the probability of transmission from one host to another. In infectious diseases of humans and animals contact structures are determined by networks of social contacts. Plant pathogens spread over global scales of countries and continents by natural means and through networks of trade and exchange (Brown and Hovmoller, 2002; Shaw and Pautasso, 2014). However, at a local scale of a single field of crop plants or several adjacent fields, plant pathogens spread primarily through passive dispersal of infectious propagules through air, water or soil

between immobile plants. Insect pests may disperse both actively and passively between hosts plants (Mazzi and Dorn, 2012). In both of these cases, the probability of transmission between hosts depends on the geographical distance between them. Hence, the contact structure is determined by the spatial scales of pathogen dispersal and the spatial scales of the host population. Full information on the contact structure is difficult to obtain and to analyze. Several global measures are used to characterize networks of contacts, such as the average degree, i. e. the average number of links per host. Yet, a better measure that characterizes the disease spread is its basic reproductive number, R_0 , defined intuitively as “the average number of secondary cases of infection generated by one primary case in a susceptible host population” (Anderson and May, 1986). Mathematically, it is given by the dominant eigenvalue of the next generation operator (Heesterbeek, 2002). Hence, the basic reproductive number is a quantity with a clear biological meaning that characterizes reproductive fitness of the pathogen. It determines the invasion threshold: if $R_0 > 1$ the disease will spread in the population, otherwise at $R_0 < 1$ the pathogen will eventually die out. Therefore, R_0 can be used to estimate the critical proportion of the host population that needs to be immunized (i. e. vaccinated) in order to eradicate the disease (Anderson and May., 1991). Also, R_0 often allows one to estimate the final (equilibrium) disease level.

Much attention has been devoted to estimation of R_0 for infectious diseases of humans and animals (Anderson and May., 1991; Fraser et al., 2009; Hampson et al., 2009). Several studies discuss R_0 in the context of infectious diseases of plants (Gubbins et al., 2000; Park et al., 2001; Parnell et al., 2005; van den Bosch et al., 2008), but only one study provided actual estimates based on measurements of the apparent infection rate r (the rate of growth of the disease proportion over time, assuming logistic growth (Vanderplank, 1963)) for wheat stripe rust (Segarra et al., 2001). Another approach is to estimate R_0 by fitting the solution of a population dynamics model of disease spread to an empirical disease progress curve (i. e. the plot of the proportion of disease over time). However, this appears to be difficult, because we expect R_0 to depend on the spatial scales of the host population. In an agricultural setting, crop plants are usually arranged in nearly rectangular fields. Each field is characterized by its area S and aspect ratio α . Hence, R_0 should depend on S and α , provided that the planting density is fixed. Given the wide variation in field sizes and shapes across individual fields and growing regions, countries and continents, a useful estimate for R_0 should also capture the dependence on the field size and shape. But measuring disease progress curves in many fields with different sizes and shapes requires enormous efforts and resources.

In this study we propose a novel way to estimate the basic reproductive number R_0 as a function of field size and shape. This approach uses a spatially explicit population dynamics model formulated as a system of integro-differential equations. The estimation of R_0 is based on disease gradient measurements in which the amount of disease is characterized as a function of the distance from a localized source of initial inoculum. The advantage of this approach is that, by measuring the disease gradient over a large enough distance in a single experiment, one captures the information on the dependence of R_0 on the field size and aspect ratio. In this way, more useful information can be extracted from disease gradient data than thought previously. To provide a proof of principle for this method, we applied it to wheat stripe rust (an important pathogen of wheat caused by *Puccinia striiformis* (Wellings, 2011)), since disease gradients for this pathogen were thoroughly measured over large distances (Sackett and Mundt, 2005a; Cowger et al., 2005). Using these data, we estimated R_0 as a function of the field size and shape.

From this dependence we determined the ranges of field sizes and shapes over which R_0 exhibits a considerable change.

2. Materials and methods

We assume that the hosts are continuously distributed across the rectangular field with the dimensions d_x and d_y . The field area is $S = d_x d_y$ and its aspect ratio is $\alpha = d_x/d_y$, so that α close to zero refers to long, narrow fields, while $\alpha = 1$ represents a square field. We trace the densities of healthy hosts $H(x, y, t)$ and infected hosts $I(x, y, t)$ in space and time using the system of integro-differential equations

$$\frac{\partial H(x, y, t)}{\partial t} = r_H H(x, y, t) [1 - H(x, y, t)/K] - \beta \lambda(x, y) H(x, y, t), \quad (1)$$

$$\frac{\partial I(x, y, t)}{\partial t} = \beta \lambda(x, y) H(x, y, t) - \mu I(x, y, t). \quad (2)$$

Here, the force of infection $\lambda(x, y)$ at a location x, y is determined by integrating over all possible sources of infection:

$$\lambda = \int_0^{d_x} du \int_0^{d_y} dv \kappa(x, y, u, v) I(u, v, t). \quad (3)$$

In obtaining Eqs. (1)-(2) we assumed that the characteristic time scale of spore dispersal is much shorter than the characteristic time scales associated with other stages of the pathogen life cycle and, hence, the density of spores is proportional to the density of the infectious host tissue (see Appendix A.4 in Supporting Information for more details).

The quantities $H(x, y, t)$ and $I(x, y, t)$ represent the areas of the corresponding host tissue per unit land area. The host tissue could be leaves, stems or grain, depending on the specific host-pathogen interaction. Healthy hosts $H(x, y, t)$ grow logistically with the rate r_H and the ‘‘carrying capacity’’ K , which may imply limited space or nutrients. Furthermore, healthy hosts may be infected by the pathogen and transformed into infected hosts with the rate $\beta \lambda(x, y)$. The transmission rate β is a compound parameter given by the product of the sporulation rate of the infected tissue and the probability that a spore causes new infection. Infected host tissue loses its infectivity at a rate μ , where μ^{-1} is the average infectious period. An approximate version of the model Eqs. (1)-(2), in which the host densities were assumed to be homogeneous in space, was used in several previous studies of plant disease epidemics (Hall et al., 2007; van den Bosch and Gilligan, 2008; Mikaberidze et al., 2014b).

The integral in Eq. (3) is weighted using $\kappa(x, y, u, v)$, the dispersal kernel (or contact distribution (Mollison, 1977)) that characterizes the dispersal properties of the pathogen. The dispersal properties as well as the environmental conditions are assumed to be the same along the field. Moreover, dispersal is assumed to be isotropic, meaning that a spore has the same probability to move in any direction along the two-dimensional field. The latter assumption can be problematic when strong winds prevail in a certain direction and may be the cause of discrepancy with the empirical findings (see Appendix A.5). In this case, the dispersal kernel is only determined by the distance between the source and the target of infection, i. e. $\kappa(x, y, u, v) = \kappa(r)$, where

$r = \sqrt{(x - u)^2 + (y - v)^2}$. For aerially dispersed plant diseases, $\kappa(r)$ is defined as a probability density function for an infectious spore to land at a distance r from its source (Nathan et al., 2012).

In order to determine the basic reproductive number, R_0 , we perform the linear stability analysis of the disease-free equilibrium of the system Eqs. (1)-(2). This leads to the eigenvalue problem for the Fredholm equation of the second kind (see Appendix A.1 for the derivation)

$$R_{0\infty} \int_0^{d_x} du \int_0^{d_y} dv \kappa(r) w(u, v) = \sigma w(x, y), \quad (4)$$

where $R_{0\infty} = \beta K / \mu$. By solving this problem, we can find the eigenvalues σ_i and eigenfunctions $w_i(x, y)$ that satisfy the Eq. (4). The dominant eigenvalue σ_d determines the basic reproductive number, i. e. $R_0 = \sigma_d$. Although an approximate expression for R_0 based on its intuitive definition may often give sound results, this cannot be guaranteed (see Appendix A.2).

3. Results

We first consider the generic features of how the basic reproductive number, R_0 , depends on the field size d . Then, we consider these dependencies in the case of wheat stripe rust in Sec. 3.2.

3.1. Dependence of the basic reproductive number on the field size

The basic reproductive number, R_0 , is shown in Fig. 1 as a function of the linear extension d of a square field for three different dispersal kernels (Gaussian, exponential and modified power-law). These three functional forms are often used to describe dispersal gradients in plant diseases (Fitt et al., 1987; Frantzen and Bosch, 2000; Sackett and Mundt, 2005a), but also in other taxonomic groups, for example, in pollen, seeds, seedlings, beetles, moths and butterflies (Nathan et al., 2012). These three functions represent the three classes of dispersal kernels: “thin-tailed” (Gaussian) that decrease faster than exponential, exponential, and “fat-tailed” that decrease slower than exponential (power-law). “Thin-tailed” and exponential kernels give rise to travelling epidemic waves with a constant velocity, while the “fat-tailed” kernels result in accelerating epidemic waves (Mollison, 1977; Medlock and Kot, 2003; Cowger et al., 2005; Sackett and Mundt, 2005b).

For all the three types of dispersal kernels that we considered, the basic reproductive number first increases as a function of the field size d and then, eventually, saturates to a constant value (Fig. 1). Thus, we find that the qualitative dependence of R_0 , a more basic epidemiological parameter than the epidemic velocity, on the field size is quite robust with respect to the functional form of the dispersal kernel. In particular, it is not affected much by the nature of the tails of the dispersal kernel. Moreover, we expect this behaviour to hold for any dispersal kernel, as long as it is a monotonically decreasing function of the distance r .

The initial growth of R_0 versus d follows a quadratic function (see Eq. (A.10)). It occurs because in this range, the field size is much smaller than the dispersal radius a (a characteristic length scale of pathogen dispersal), i. e. $d \ll a$. Therefore, by making the field larger, more spores will land within the field and lead to new infections. In other words, in this range the field size is the

limiting factor for the pathogen fitness. On the contrary, when the field size is much larger than the dispersal radius, i. e. $d \gg a$, the basic reproductive number becomes independent of d . Here, pathogen does not become fitter on a larger field, because its fitness is now limited by the range of dispersal and not by the size of the field.

While the three curves in Fig. 1 exhibit a universal qualitative behaviour, they differ in the rate at which the saturation occurs at large field sizes. The Gaussian dispersal kernel decreases faster with the distance r than the exponential dispersal kernel. As a result, R_0 grows and saturates as a function of the field size d faster for the Gaussian than for the exponential. The result for the power-law dispersal kernel is difficult to compare with the results for other kernels, since the power law lacks a meaningful characteristic length scale. Asymptotically, at large field sizes R_0 approaches the constant value slower in the case of the power-law dispersal kernel than for the other two kernels. However, at small field sizes, R_0 as a function of d may grow faster or slower for the power-law kernel as compared to the other two kernels, depending on the values of the parameters r_0 and b . In Fig. 1, we present an example when the R_0 for the power law first grows faster than the that for the Gaussian or exponential dispersal kernels, but subsequently its growth slows down and becomes slower than for the Gaussian and exponential (as expected from the asymptotic behavior of the corresponding dispersal kernels).

3.2. Case study: dependence of the basic reproductive number on the field size and shape for wheat stripe rust

We infer the dependence of the basic reproductive number, R_0 , on the field size and shape from the detailed measurements of primary disease gradients of wheat stripe rust (Sackett and Mundt, 2005a; Cowger et al., 2005). R_0 is computed by numerically solving the eigenvalue problem in Eq. (4) for different values of the field dimensions d_x and d_y that characterize the field size and shape. To perform this calculation, we estimated the dispersal kernel $\kappa(r)$ and the compound parameter $R_{0\infty}$ that corresponds to the basic reproductive number for a very large field from experimental data (Sackett and Mundt, 2005a; Cowger et al., 2005) [see Appendix A.3 for the details of the estimation procedure].

In these experiments, small areas of experimental plots (foci) were artificially inoculated by pathogen spores (0th generation). These spores give rise to lesions in the focus (first generation) that further produce spores, which are dispersed through the air. This gives rise to infection outside of the focus, producing the second generation of pathogen lesions. The corresponding disease severity (the proportion of the leaf area infected) is measured as a function of the distance r from the focus.

The outcome of this measurement is shown in Fig. 2 for the two largest datasets (Hermiston 2002 and Madras 2002, downwind) obtained in this experiment. These two datasets were chosen because they contained measurements over large enough distances that allowed us to obtain sound fits. Disease severity strongly depends on the distance r : the value is largest closer to the focus and decreases monotonically with r . The data can be fitted well by the modified power-law function (solid curve in Fig. 2)

$$\kappa_{\text{PL2}}(r) = \kappa_0 (r_0^2 + r^2)^{-b/2}. \quad (5)$$

In contrast, exponential and Gaussian functions provide poor fits (dashed and dotted curves in

Fig. 2). (For more details on fitting see Appendix A.3.1 and Fig. 6 in the Electronic Supplementary Materials).

Disease gradients, measured in this way, contain information on the three key processes in the pathogen life-cycle: spore production, aerial movement of spores, and infection of healthy host tissue. We assume that the rate of spore production and the probability to infect healthy host tissue, once the spore has landed on it, are homogeneous across the field, i. e. do not depend on the distance r . Hence, the compound parameter $R_{0\infty} = \beta K/\mu$ that characterizes these processes does not depend on the distance. Therefore, the aerial movement of spores is the only process that depends on the distance r . Further, we assume that there is a large enough number of spores produced and the probability of infection is large enough such that the recorded disease severity is proportional to the spore concentration in the air. Under these assumptions, our estimate for the dispersal kernel $\kappa(r)$ is the modified power-law function [Eq. (5)] fitted to the disease gradient data and normalized as a probability density function (i. e. such that its integral over the whole two-dimensional space equals to unity [Appendix A.3.2]). We also estimated the parameter $R_{0\infty}$ from the disease gradient data (see Appendix A.3.3) and obtained the value $R_{0\infty} = 65.0$ for the Hermiston 2002 downwind dataset; and the value $R_{0\infty} = 38.0$ for the Madras 2002 downwind dataset.

Using our estimates for the dispersal kernel, $\kappa(r)$, and the parameter $R_{0\infty}$ we solved the eigenvalue problem Eq. (4) numerically for different field sizes and shapes. In this way, we obtained the dependence of the basic reproductive number R_0 on the field size (Fig. 3) and its aspect ratio (Fig. 4). In Fig. 3, R_0 first grows steeply versus the linear extension of a square field and saturates towards the asymptotic value $R_{0\infty}$ for large fields. The basic reproductive number is about two times larger for the parameter values corresponding to Hermiston 2002 dataset, than for the case of Madras 2002 dataset. This difference stems from the difference in the asymptotic values $R_{0\infty}$ and also from different shapes of the disease gradients (cf. panel (a) and (b) in Fig. 2). The asymptotic value, $R_{0\infty}$, (indicated by the horizontal dashed line in Fig. 3), is approached faster in the case of Hermiston 2002 dataset (solid curve in Fig. 3), than for Madras 2002 dataset (dashed curve in Fig. 3). The reason for this is a different exponent of the power-law function that best fits the corresponding disease gradients ($b = 3.04$ for Hermiston 2002, Eq. (A.15), and $b = 2.23$, Eq. (A.16)). The disease gradient in Madras 2002 decreases slower due a lower exponent.

In Fig. 4, R_0 exhibits a saturating growth as the field aspect ratio α is increased from 0.01 to 1. Hence, the square fields, with $\alpha = 1$, are most conducive for the disease growth. The basic reproductive number grows faster and saturates at larger values of α in smaller fields (cf. dotted, dashed, dash-dotted and solid curves in Fig. 4).

A number of empirical studies have reported that, in agreement with our results, smaller plots resulted in lower disease levels in wheat yellow rust (Mundt et al., 1996), wheat brown rust (*Puccinia recondita* f. sp. *tritici*) (Bowen et al., 1984), potato late blight (Paysour and Fry, 1983) and *Valdensia heterodoxa* on *Vaccinium myrtillus* (Strengbom et al., 2006). However, in a more recent study in wheat yellow rust (Sackett and Mundt, 2009) that used considerably larger plot sizes, the plot size did not affect the epidemic velocity. Our estimation framework predicts moderate differences in the values of R_0 between larger square plots and smaller elongated plots used in experiments (Sackett and Mundt, 2009) (cf. the white and gray circles in both panels of Fig. 4). This is expected to result in higher epidemic velocities in larger plots compared to smaller plots, according to theoretical arguments (see Appendix A.5). We suggest two possible

explanations for this discrepancy (see Appendix A.5 for more details). First, strong wind with a prevailing direction along the axis of the elongated plot was observed in the experimental setting (Sackett and Mundt, 2009), but in our model isotropic dispersal was assumed. The differences in R_0 between smaller elongated plot and a larger square plot that we predict using the model are possibly masked by the wind. This is because the wind may increase the pathogen's R_0 in the smaller elongated plot by preventing the spores to land outside the plot. Second, a moderate difference of 20-30 % that we predict for epidemic velocities may be difficult to detect given the level of experimental uncertainties.

4. Discussion

We found that the basic reproductive number, R_0 , of crop pathogens depends on the size and geometry of the field planted with host plants. R_0 increases with the field size at small field sizes and saturates to a constant values at large field sizes. The value of R_0 reaches its maximum in square fields and decreases as the field becomes elongated, while retaining the same area. This pattern appears to be quite general: it holds for dispersal kernels that decrease exponentially or faster (i. e. Gaussian kernels) as well as for “fat-tailed” dispersal kernels that decrease slower than exponential ones (i. e. power-law kernels). We expect the same qualitative behavior for any dispersal kernel, provided that it is a monotonically decreasing function of the distance.

As expected, this qualitative picture also holds for the dispersal kernels estimated in wheat stripe rust. The asymptotic values of the basic reproductive number at large field sizes ($R_{0\infty} = 65.0$ for Hermiston 2002 downwind, $R_{0\infty} = 38.0$ for the Madras 2002 downwind dataset) result in the values of the apparent rate of infection $r \approx 0.21$ for Hermiston and $r \approx 0.18$ for Madras, where the simple relationship $r = \mu \log R_0$ was used. These values are quite close to the estimates of r obtained independently for these experiments ($r \approx 0.25$ (Cowger et al., 2005)). Also, in (Segarra et al., 2001) the R_0 of wheat yellow rust was estimated to be around 60 from the measurements of the apparent rate of infection r . This study used a more rigorous approach to connect r and R_0 that took into account the shape of the sporulation curve. Our estimates of $R_{0\infty}$ are also consistent, but somewhat smaller than the estimates from field experiments, where the number of secondary lesions originating from a single lesion was measured to be as high as several hundred (Farber et al., 2013).

The estimates for $R_{0\infty}$ that we obtained for wheat stripe rust are considerably larger than typical estimates for the basic reproductive number for human or animal diseases. For example, the relatively large values of R_0 were estimated for childhood diseases such as measles (14-18) and pertussis (5-18) (Anderson and May., 1991), the estimates for the “swine flu” influenza H1N1 were in the range 1.4-1.6 (Fraser et al., 2009), the estimates for rabies were in the range 1-2 (Hampson et al., 2009). A possible exception is malaria, where the estimates of R_0 between one and more than 3000 were reported (Smith et al., 2007). The R_0 determines the critical proportion p_c of the host population that needs to be immunized in order to eradicate the disease ($p_c = 1 - 1/R_0$) (Anderson and May., 1991). For example, our estimate for the wheat stripe rust of $R_0 \simeq 50$ yields the critical proportion $p_c \simeq 0.98$. This may explain why it is so difficult to eradicate rusts, while there are cases of dangerous human diseases (for example, small pox) that were eradicated with the help of vaccination programmes (Anderson and May., 1991). This difference in the values of R_0 may result from a different biology of hosts (animals versus plants),

or, alternatively, it could be due to different nature of the diseases, i. e. systemic diseases in the case of humans and animals versus local lesion diseases in the case of wheat stripe rust. To determine which of these two explanations is more plausible, one needs to estimate R_0 for systemic disease of plants and local lesion (i. e. skin diseases) of animals. This difference may also be caused by the characteristic features of host populations in agroecosystems, where genetically uniform hosts are planted with high densities in a homogeneous environment. Hence, it would be interesting to compare the R_0 of crop pathogens with the R_0 of plant pathogens in natural ecosystems.

These findings can be used to control plant diseases, if one knows the spatial scales, i. e. field sizes and aspect ratios, over which R_0 changes considerably. We found that the R_0 of wheat stripe rust exhibits a large change at a fine spatial scale: when the linear dimension of a square field increases from zero to about thirty meters (Fig. 3). The most substantial change of R_0 as a function of the field aspect ratio occurs between aspect ratios of 0.01 and 0.2. These results suggest, that decreasing field sizes and elongating fields may not be a practical measure to control wheat stripe rust, because the beneficial effect of lowering the disease levels is in this case unlikely to outweigh the economical costs associated with using smaller and longer fields. But this method could be feasible for controlling other diseases of crops or pests (for example, western corn rootworm that can disperse over longer distances (Carrasco et al., 2010) than wheat stripe rust). We hope that our study will stimulate more detailed empirical studies of the disease gradients for different crop pathogens over long distances, such that the framework proposed here could be used to infer how the R_0 depends on the spatial scales of the host population. Although similar ideas about possibilities to control plant diseases by adjusting field size and geometry were explored mathematically in (Fleming et al., 1982), their framework based on reaction-diffusion models was not capable of including realistic dispersal kernels. Hence, they could not estimate the spatial scales at which the pathogen fitness changes considerably.

The experiments in Hermiston 2002 and Madras 2002 used the same planting density, the same wheat cultivar and the same pathogen race was used for initial inoculation. But the environmental conditions were somewhat different in these two locations. Hence, we can largely attribute the difference in the disease gradients between these two datasets and the resulting difference in the estimated values of the basic reproductive number to the difference in the environmental conditions. In contrast, in natural epidemics the variation in the outcomes of pathogen dispersal can also result from the genetic variation in pathogen and host population (Tack et al., 2013). Therefore, it would be interesting to explore the effect of simultaneously adjusting the spatial scales and introducing genetic diversity to the host population by using host mixtures or multiline cultivars (Mundt, 2002; Mikaberidze et al., 2014a)

From another point of view, our findings could be helpful for choosing the minimum plot sizes and aspect ratios for field experimentation in plant pathology. For the experimental plots to be representative of larger fields used by growers, the plot size and aspect ratio should be chosen such that they correspond to the start of the saturation of the dependency of R_0 on the field size (Fig. 3) and aspect ratio (Fig. 4). Thus, our results indicate that in the case of wheat stripe rust, the area of experimental plots should be at least 0.25 ha and the aspect ratio should be at least 0.2 (this corresponds approximately to a 20 m \times 110 m elongated plot, or, alternatively, a 50 m \times 50 m square plot).

Our results could also help to manage fungicide resistance: if several different fungicides are applied over smaller, elongated patches within a larger field, then the fitness of resistant strains

would be diminished. This strategy allows one to keep the overall field size large enough to be economically advantageous, but requires availability of several different fungicides that have little or no cross-resistance. The same reasoning applies also for the case of break-down of disease resistance in host plants. In this case, host cultivars with different disease resistances should be arranged in smaller, elongated patches within a larger field. Favorable arrangements of these patches with different fungicides and host cultivars that would reduce selection for fungicide resistance and minimize break-down of host defences can be investigated using dynamical simulations of the population dynamics model based on Eqs. (1)-(2). In order to suggest economically viable implementations, an epidemiological modeling framework should be coupled with a sound economical cost-benefit analysis.

So far we discussed disease control on the level of a single field of crops. But our study also provides a way to incorporate the dependence of R_0 on the spatial structure of the local host population into models of disease spread on a regional scale (such as the models described in (Parnell et al., 2006; Papaix et al., 2014)). In this context we expect the nature of tails of the dispersal kernels to play an important role in the disease spread and would influence optimal strategies of disease control.

5. Acknowledgements

AM and SB gratefully acknowledge financial support by the ERC advanced grant PBDR 268540 “The population biology of drug resistance: Key principles for a more sustainable use of drugs”. The contributions of CM were supported by NIH grant R01GM96685 through the NSF/NIH Ecology and Evolution of Infectious Disease Program. The authors would like to thank Kathryn Sackett for providing estimates of the apparent infection rate and helpful discussions. AM is grateful to Bruce McDonald and Roland Regoes for many valuable discussions.

References

- Anderson, R. M., and R. M. May. 1986. The invasion, persistence and spread of infectious diseases within animal and plant communities. *Philosophical transactions of the Royal Society of London. Series B, Biological sciences* **314**:533–70.
- Anderson, R. M., and R. M. May. 1991. *Infectious diseases of humans*. Oxford University Press.
- Bowen, K., P. Teng, and A. Roelfs. 1984. Negative Interplot Interference in Field Experiments with Leaf Rust of Wheat. *Phytopathology* **74**:1157–61.
- Brown, J. K. M., and M. S. Hovmoller. 2002. Aerial dispersal of pathogens on the global and continental scales and its impact on plant disease. *Science (New York, N.Y.)* **297**:537–41.
- Carrasco, L., T. Harwood, S. Toepfer, A. MacLeod, N. Levay, J. Kiss, R. Baker, J. Mumford, and J. Knight. 2010. Dispersal kernels of the invasive alien western corn rootworm and the effectiveness of buffer zones in eradication programmes in Europe. *Annals of Applied Biology* **156**:63–77.

- Cowger, C., L. D. Wallace, and C. C. Mundt. 2005. Velocity of spread of wheat stripe rust epidemics. *Phytopathology* **95**:972–82.
- Diekmann, O., J. A. P. Heesterbeek, and J. A. J. Metz. 1990. On the definition and the computation of the basic reproduction ratio R_0 in models for infectious diseases in heterogeneous populations. *Journal of Mathematical Biology* **28**:365–382.
- Farber, D., L. Estep, K. Sackett, and C. Mundt. 2013. Local dispersal of *Puccinia striiformis* f.sp. *tritici* from single source lesions. *Phytopathology APS-MSA Joint Meeting, Austin TX* **103**:41.
- Fitt, B. D. L., P. H. Gregory, a. D. Todd, H. a. McCartney, and O. C. Macdonald. 1987. Spore Dispersal and Plant Disease Gradients; a Comparison between two Empirical Models. *Journal of Phytopathology* **118**:227–242.
- Fleming, R., L. Marsh, and H. Tuckwell. 1982. Effect of field geometry on the spread of crop disease. *Protection Ecology* **4**:81.
- Frantzen, J., and F. V. D. Bosch. 2000. Spread of organisms: can travelling and dispersive waves be distinguished ? *Basic and Applied Ecology* **91**:83–91.
- Fraser, C., C. a. Donnelly, S. Cauchemez, W. P. Hanage, M. D. Van Kerkhove, T. D. Hollingsworth, J. Griffin, R. F. Baggaley, H. E. Jenkins, E. J. Lyons, T. Jombart, W. R. Hinsley, N. C. Grassly, F. Balloux, A. C. Ghani, N. M. Ferguson, A. Rambaut, O. G. Pybus, H. Lopez-Gatell, C. M. Alpuche-Aranda, I. B. Chapela, E. P. Zavala, D. M. E. Guevara, F. Checchi, E. Garcia, S. Hugonnet, and C. Roth. 2009. Pandemic potential of a strain of influenza A (H1N1): early findings. *Science (New York, N.Y.)* **324**:1557–61.
- Gregory, P. 1968. Interpreting plant disease dispersal gradients. *Annual Review of Phytopathology* **6**:189.
- Gubbins, S., C. A. Gilligan, and A. Kleczkowski. 2000. Population dynamics of plant-parasite interactions: thresholds for invasion. *Theoretical Population Biology* **57**:219–33.
- Hall, R. J., S. Gubbins, and C. A. Gilligan. 2007. Evaluating the performance of chemical control in the presence of resistant pathogens. *Bulletin of mathematical biology* **69**:525–37.
- Hampson, K., J. Dushoff, S. Cleaveland, D. T. Haydon, M. Kaare, C. Packer, and A. Dobson. 2009. Transmission dynamics and prospects for the elimination of canine rabies. *PLoS Biology* **7**:e53.
- Heesterbeek, J. 2002. A Brief History of R_0 and a Recipe for its Calculation. *Acta Biotheoretica* **5**:189–204.
- Keeling, M. J., and P. Rohani, 2008. Spatial Models. Chapter 7, page 266 *in* *Modeling Infectious Diseases in Humans and Animals*. Princeton University Press, Princeton.
- Lambert, D. H., R. L. Villareal, D. R. Mackenzie, and T. P. Agri. 1980. A General Model for Gradient Analysis. *Phytopathol. Z.* **154**:150–155.

- Mazzi, D., and S. Dorn. 2012. Movement of insect pests in agricultural landscapes. *Annals of Applied Biology* **160**:97–113.
- McDonald, B. A., and C. Linde. 2002. Pathogen population genetics, evolutionary potential, and durable resistance. *Annual Review of Phytopathology* **40**:349–79.
- Medlock, J., and M. Kot. 2003. Spreading disease: integro-differential equations old and new. *Mathematical Biosciences* **184**:201–222.
- Mikaberidze, A., B. McDonald, and S. Bonhoeffer. 2014a. How to develop smarter host mixtures to control plant disease? *arXiv:1402.2788*.
- Mikaberidze, A., B. A. McDonald, and S. Bonhoeffer. 2014b. Can high risk fungicides be used in mixtures without selecting for fungicide resistance? *Phytopathology* **104**:324–331.
- Mollison, D. 1977. Spatial Contact Models for Ecological and Epidemic Spread. *Journal of the Royal Statistical Society. Series B* **39**:283.
- Mundt, C., and K. Leonard. 1985. A modification of Gregory's model for describing plant disease gradients. *Phytopathology* **75**:930.
- Mundt, C. C. 2002. Use of multiline cultivars and cultivar mixtures for disease management. *Annual review of phytopathology* **40**:381–410.
- Mundt, C. C. 2014. Durable resistance: A key to sustainable management of pathogens and pests. *Infection, genetics and evolution: journal of molecular epidemiology and evolutionary genetics in infectious diseases* **in press**.
- Mundt, C. C., L. S. Brophy, and S. C. Kolar. 1996. Effect of genotype unit number and spatial arrangement on severity of yellow rust in wheat cultivar mixtures. *Plant Pathology* **45**:215–222.
- Nathan, R., E. Klein, J. J. Robledo-Arnuncio, and E. Revilla, 2012. Dispersal kernels: review. Chapter 15, page 187 *in* J. Clobert, M. Baguette, T. G. Benton, and J. M. Bullock, editors. *Dispersal ecology and evolution*. Oxford Univ. Press.
- Papaix, J., S. Touzeau, H. Monod, and C. Lannou. 2014. Can epidemic control be achieved by altering landscape connectivity in agricultural systems? *Ecological Modelling* **284**:35–47.
- Park, A. W., S. Gubbins, and C. A. Gilligan. 2001. Invasion and persistence of plant parasites in a spatially structured host population. *Oikos* **94**:162–174.
- Parnell, S., C. a. Gilligan, and F. van den Bosch. 2005. Small-scale fungicide spray heterogeneity and the coexistence of resistant and sensitive pathogen strains. *Phytopathology* **95**:632–9.
- Parnell, S., F. van den Bosch, and C. a. Gilligan. 2006. Large-scale fungicide spray heterogeneity and the regional spread of resistant pathogen strains. *Phytopathology* **96**:549–55.
- Paysour, R., and W. Fry. 1983. Interplot interference: A model for planning field experiments with aerielly disseminated pathogens. *Phytopathology* **73**:1014.

- Press, W. H., S. A. Teukolsky, W. T. Vetterling, and B. P. Flannery, 1992. Chapter 18. Integral Equations and Inverse Theory. Page 788 in *Numerical Recipes in C*. Cambridge University Press, Cambridge.
- Sackett, K. E., and C. C. Mundt. 2005*a*. Primary disease gradients of wheat stripe rust in large field plots. *Phytopathology* **95**:983–91.
- Sackett, K. E., and C. C. Mundt. 2005*b*. The effects of dispersal gradient and pathogen life cycle components on epidemic velocity in computer simulations. *Phytopathology* **95**:992–1000.
- Sackett, K. E., and C. C. Mundt. 2009. Effect of plot geometry on epidemic velocity of wheat yellow rust. *Plant Pathology* **58**:370–377.
- Segarra, J., M. J. Jeger, and F. van den Bosch. 2001. Epidemic dynamics and patterns of plant diseases. *Phytopathology* **91**:1001–10.
- Shaw, M. W., and M. Pautasso. 2014. Networks and Plant Disease Management: Concepts and Applications. *Annual Review of Phytopathology* **52**:in press.
- Smith, D. L., F. E. McKenzie, R. W. Snow, and S. I. Hay. 2007. Revisiting the basic reproductive number for malaria and its implications for malaria control. *PLoS Biology* **5**:e42.
- Strange, R. N., and P. R. Scott. 2005. Plant disease: a threat to global food security. *Annual Review of Phytopathology* **43**:83–116.
- Strengbom, J., G. Englund, and L. Ericson. 2006. Experimental scale and precipitation modify effects of nitrogen addition on a plant pathogen. *Journal of Ecology* **94**:227–233.
- Tack, A., J. Hakala, T. Petäjä, M. Kulmala, and A. Laine. 2013. Genotype and spatial structure shape pathogen dispersal and disease dynamics at small spatial scales. *Ecology* **95**:703–714.
- van den Bosch, F., and C. A. Gilligan. 2008. Models of fungicide resistance dynamics. *Annu. Rev. Phytopathol.* **46**:123–47.
- van den Bosch, F., N. McRoberts, F. van den Berg, and L. Madden. 2008. The Basic Reproduction Number of Plant Pathogens: Matrix Approaches to Complex Dynamics. *Phytopathology* **98**:239–249.
- Vanderplank, J. E. 1963. *Plant Diseases: Epidemics and Control*. Academic Press, New York.
- Wellings, C. R. 2011. Global status of stripe rust: a review of historical and current threats. *Euphytica* **179**:129–141.

Table 1: Variables and parameters

	Description	Dimension
Variables		
$H(x, y, t)$	Density of healthy host tissue	dl
$I(x, y, t)$	Density of infected host tissue	dl
Parameters		
d_x, d_y	Linear dimensions of the field along x and y	m
a	Characteristic spatial scale of pathogen dispersal (dispersal radius)	m
β	Transmission rate	days ⁻¹
μ^{-1}	Average infectious period	days
r_H	Growth rate of healthy host tissue	days ⁻¹
K	“Carrying capacity” of the healthy host tissue	dl
$R_{0\infty}$	Basic reproductive number in the limit of a very large field	dl
Functions		
$\kappa(r)$	Dispersal kernel	m ⁻¹
$R_0(d_x, d_y)$	Basic reproductive number	dl
$\lambda(x, y)$	The force of infection [Eq. (3)]	

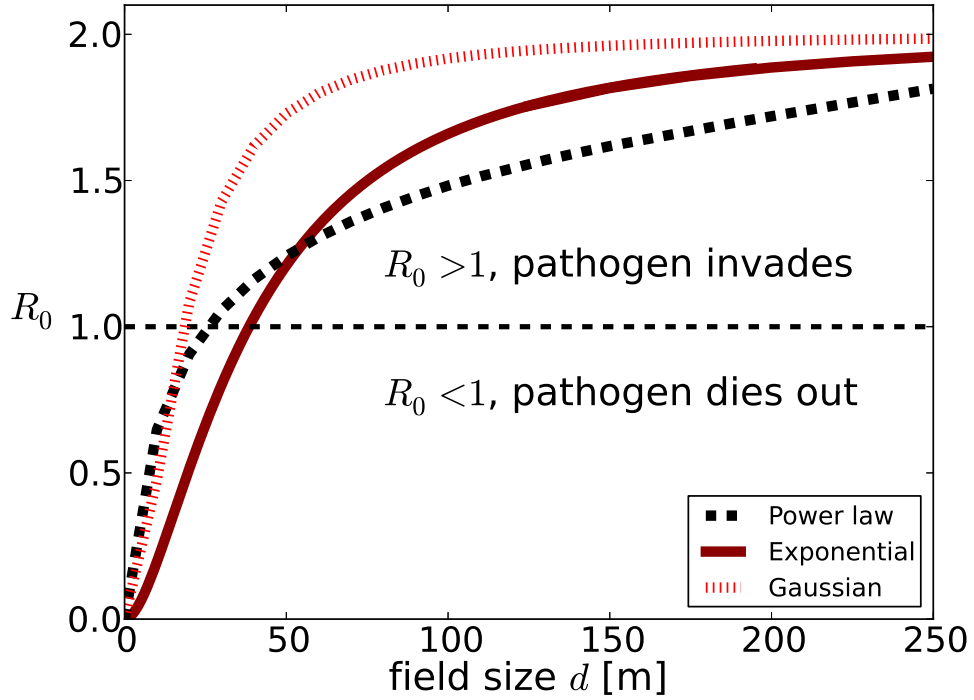


Figure 1: Basic reproductive number R_0 as a function of the field size d for the two-dimensional field according to the numerical solution of Eq. (4) (solid green) using (i) the Gaussian [Eq. (A.21) at $n = 2$, $a = 10$ m], (ii) the exponential [Eq. (A.21) at $n = 1$, $a = 10$ m] and (iii) the power law dispersal kernel [Eq. (A.19) at $r_0 = 1$ m, $b = 2.1$]. Model parameters: $R_{0\infty} = \beta K / \mu = 2$.

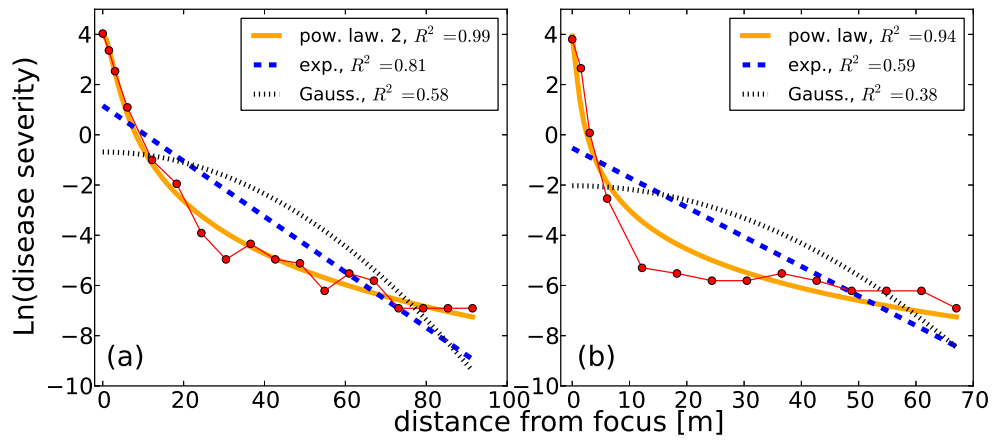


Figure 2: Disease severity of wheat stripe rust is plotted as a function of the distance from focus, outcome of field experiments (Sackett and Mundt, 2005a; Cowger et al., 2005). Two datasets, Hermiston 2002 downwind (left panel) and Madras 2002 downwind were fitted with the exponential function [Eq. (A.21) with $n = 1$, dashed curve], the Gaussian function [Eq. (A.21) with $n = 2$, dotted curve] and the modified power-law function [Eq. (A.19), solid curve].

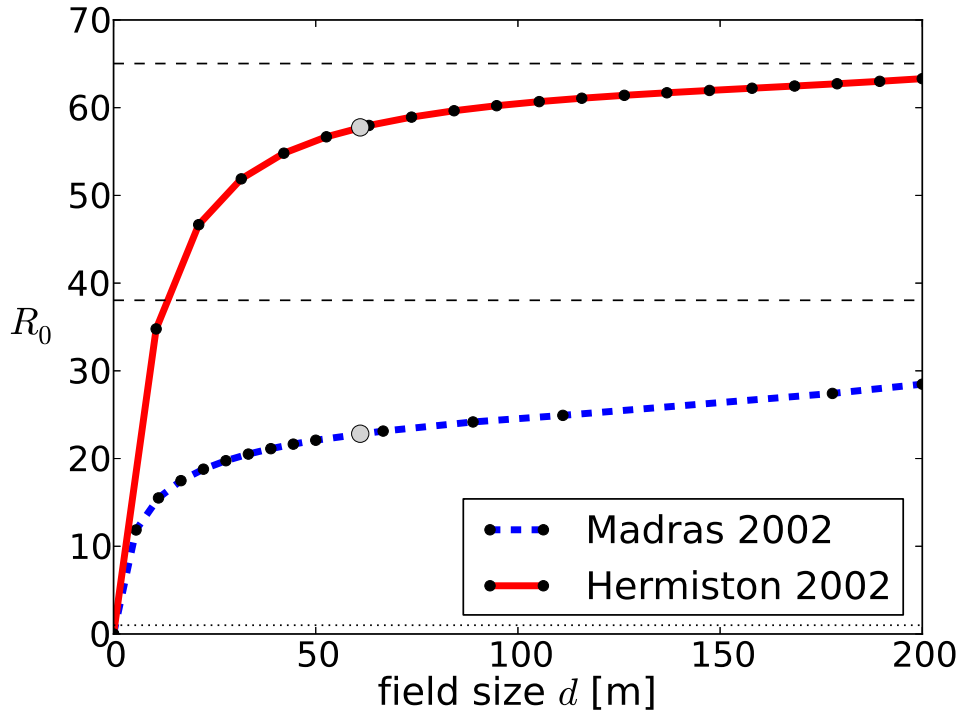


Figure 3: Basic reproductive number R_0 as a function of the field size d of a square field calculated [by solving numerically the eigenvalue problem Eq. (4)] using the modified power-law dispersal kernel [Eq. (5)] fitted in Fig. 2 to disease gradient datasets (i) Hermiston 2002 downwind (solid curve), and (ii) Madras 2002 downwind (dashed curve) obtained in (Sackett and Mundt, 2005a; Cowger et al., 2005). Horizontal dashed lines show the asymptotic values of the basic reproductive number at large field sizes, $R_{0\infty}$, for Hermiston 2002 (upper line) and Madras 2002 (lower line) datasets. Grey circles indicate the R_0 -values for the field size ($61 \text{ m} \times 61 \text{ m}$) used in the experiments (Sackett and Mundt, 2009).

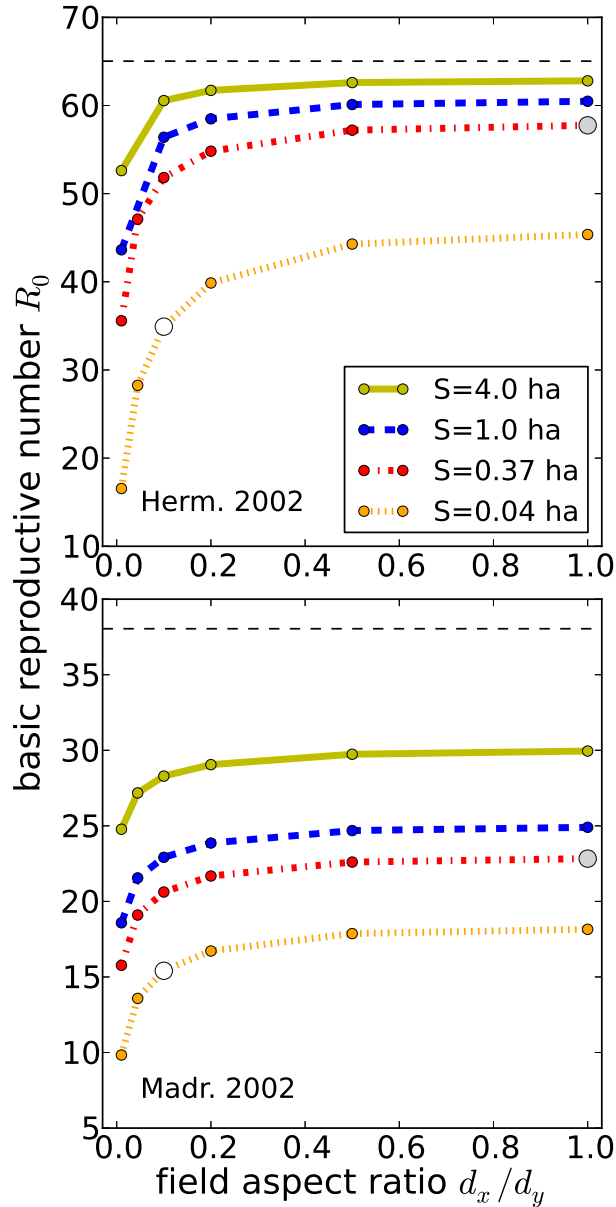


Figure 4: Basic reproductive number R_0 as a function of the field aspect ratio d_x/d_y (the field area $S = d_x d_y$ was kept the same). The calculation was performed numerically using the power-law dispersal kernels fitted to disease gradient data (Fig. 2) from Hermiston 2002 (upper panel) and Madras 2002 (lower panel) datasets obtained in (Sackett and Mundt, 2005a; Cowger et al., 2005). Different curves show the R_0 for different field areas: $S = 4$ ha (yellow solid), $S = 1$ ha (blue dashed), $S = 0.37$ ha (red dash-dotted), $S = 0.04$ ha (orange dotted). Larger circles mark the parameters at which the field experiments (Sackett and Mundt, 2009) were performed (grey circles for $6.1 \text{ m} \times 61 \text{ m}$ and white circles for $61 \text{ m} \times 61 \text{ m}$).

A. Supporting Information

A.1. Linear stability analysis of the disease-free equilibrium

We linearize the model Eqs. (1)-(2) in the vicinity of the disease-free fixed point $H(x, y, t) = K$, $I(x, y, t) = 0$ and obtain the following equations for the small deviations from this fixed point $\xi(x, y, t)$ and $I(x, y, t)$:

$$\frac{\partial \xi(x, y, t)}{\partial t} = -r_H \xi(x, y, t) - \beta K \int \kappa(x, y, u, v) I(u, v, t) du dv, \quad (\text{A.1})$$

$$\frac{\partial I(x, y, t)}{\partial t} = \beta K \int \kappa(x, y, u, v) I(u, v, t) du dv - \mu I(x, y, t). \quad (\text{A.2})$$

The disease-free fixed point becomes unstable if the small deviation $I(x, y, t)$ grows over time. To check this, we substitute $I(x, y, t) = w(x, y)e^{\lambda t}$ in Eq. (A.2). Then, the stability of the disease-free fixed point is determined by solving eigenvalue problem

$$\frac{\beta K}{\mu} \int_0^{d_x} du \int_0^{d_y} dv \kappa(r) w(u, v) = \sigma w(x, y), \quad (\text{A.3})$$

where $\sigma = 1 + \lambda/\mu$. The eigenvalue problem here consists in finding the values of λ_j and functions $w(x, y)$ satisfying the relationship (A.3). The disease-free fixed point is unstable if at least one of λ_j has a positive real part. Eq. (4) is the homogeneous Fredholm equation of the second kind and can be solved numerically using the Nystrom method (Press et al., 1992). The dominant eigenvalue σ_d determines the basic reproductive number, i. e. $R_0 = \sigma_d$. Note that the eigenvalue problem Eq. (A.3) also determines the stability properties of the corresponding integro-difference system of equations in discrete time.

A.2. Approximation for the basic reproductive number

Approximate expression for the basic reproductive number for the model Eqs. (1)-(2) can be found by applying its intuitive definition “the average number of secondary cases of infection generated by one primary case in a susceptible host population” (Anderson and May, 1986) with the averaging performed over the spatial coordinates. This leads to the expression:

$$R_{0c}(x_0, y_0) = \frac{\beta K}{\mu} \int_0^{d_x} dx \int_0^{d_y} dy \kappa(x, y, x_0, y_0). \quad (\text{A.4})$$

Here, the basic reproductive number depends on the position x_0, y_0 of the initial inoculum. The basic reproductive number in Eq. (A.4) does not yield the invasion threshold at $R_{0c}(x_0, y_0) = 1$ (Diekmann et al., 1990). However it may serve as a useful approximate expression, since the calculation according to Eq. (A.4) is often much simpler than the solution of the eigenvalue problem Eq. (A.3). In order to determine how good this approximation is, we obtain an explicit expression

for $R_{0c}(x_0, y_0)$

$$R_{0c}(x_0, y_0) = \frac{\beta K}{4\mu} \left[\operatorname{erf} \left(\frac{d_x - x_0}{\sqrt{2}d} \right) + \operatorname{erf} \left(\frac{x_0}{\sqrt{2}d} \right) \right] \left[\operatorname{erf} \left(\frac{d_y - y_0}{\sqrt{2}d} \right) + \operatorname{erf} \left(\frac{y_0}{\sqrt{2}d} \right) \right], \quad (\text{A.5})$$

where we substituted $\kappa(r)$ in Eq. (A.4) with the Gaussian dispersal kernel

$$\kappa_G(r) = \kappa_{0G} \exp[-(r/a)^2]. \quad (\text{A.6})$$

The approximate basic reproductive number $R_{0c}(x_0, y_0)$ in Eq. (A.4) depends on the position of the initial inoculum x_0, y_0 . In order to obtain a single quantity for a particular spatial configuration of the host population, we average $R_{0c}(x_0, y_0)$ over all possible values of x_0, y_0 within the field:

$$\langle R_{0c}(x_0, y_0) \rangle_{x,y} = \int_0^{d_x} dx \int_0^{d_y} dy R'_0(x, y). \quad (\text{A.7})$$

In the case of the Gaussian dispersal kernel the Eq. (A.7) yields:

$$\langle R_{0c}(x_0, y_0) \rangle_{x_0, y_0} = \frac{d^2}{d_x d_y} \frac{\beta K}{\mu} \left(\sqrt{\frac{2}{\pi}} (\exp[-d_x^2/(2a^2)] - 1) + \frac{d_x}{a} \operatorname{erf} \left[\frac{d_x}{\sqrt{2}a} \right] \right) \times \quad (\text{A.8})$$

$$\left(\sqrt{\frac{2}{\pi}} (\exp[-d_y^2/(2a^2)] - 1) + \frac{d_y}{a} \operatorname{erf} \left[\frac{d_y}{\sqrt{2}a} \right] \right). \quad (\text{A.9})$$

In Figure A.1, the approximate basic reproductive numbers $R_{0c}(x_0, y_0)$ calculated using Eq. (A.5) (dotted curves), the spatially averaged $\langle R_{0c}(x_0, y_0) \rangle_{x_0, y_0}$ [Eq. (A.8), dashed curve] and the exact basic reproductive number obtained by solving Eq. (A.3) (solid curve) are plotted versus the field size d . The approximate $R_{0c}(x_0, y_0)$ is highest when the initial inoculum is introduced to the center of the field (upper dotted curve in Fig. A.1) and is lower at the field border and in its corner (middle and lower dotted curves in Fig. A.1). The spatial averaged $\langle R_{0c}(x_0, y_0) \rangle_{x_0, y_0}$ is reasonably close to the actual R_0 (cf. dashed and solid curves in Fig. A.1), but it underestimates the actual R_0 , because it neglects the contribution of the subsequent generations of infection. At $d \gg a$ the R_0 tends asymptotically to the maximal value of $R_{0c}(x_0, y_0)$, achieved at the field center $x = d/2, y = d/2$. The values of $R_{0c}(x_0, y_0)$ at the border and in the corner of the field also reach constant but considerably smaller values at $d \ll a$. This can be explained by the fact that when the size of the field increases, the surface-to-volume ratio of the square field decreases, meaning that the contribution of the hosts close to the field border to R_0 steadily decreases.

All the curves in Fig. A.1 behave in the same way at small field sizes (i. e. when $d \ll a$): they increase quadratically with the field size d , according to

$$R_{0\text{asympt}} = \frac{\beta K}{2\pi a^2 \mu} d^2. \quad (\text{A.10})$$

Thus, the approximate expression for the basic reproductive number Eq. (A.4) holds well in the two limiting cases: at small field sizes (i. e. when $d \ll a$) and at large field sizes (i. e. when $d \gg a$).

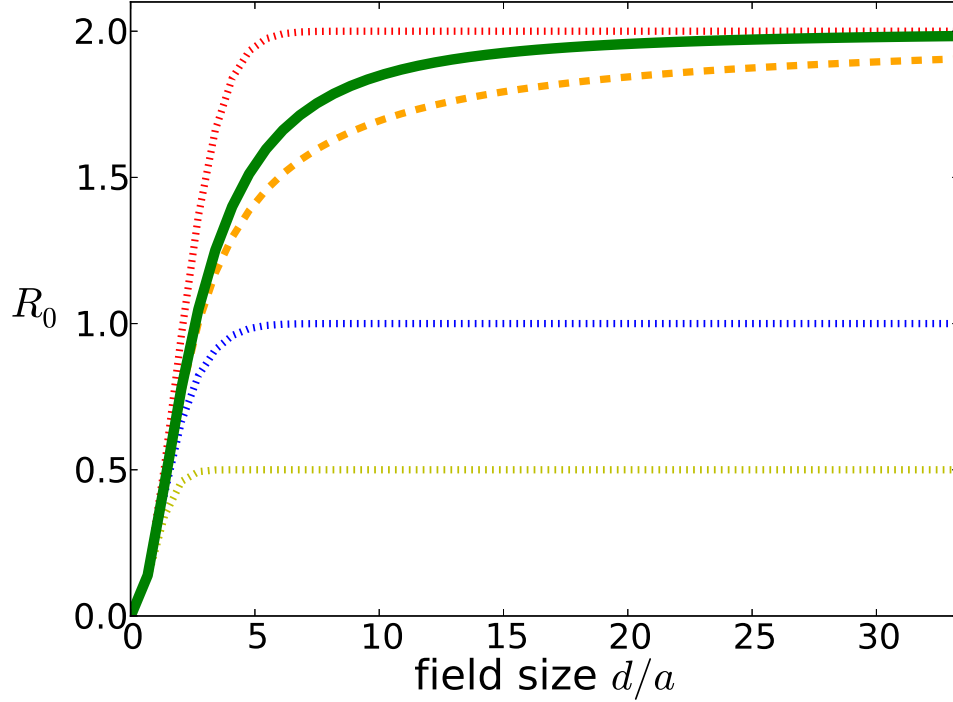


Figure A.1: Basic reproductive number R_0 as a function of the field size d of the square two-dimensional field measured in units of the dispersal radius for the Gaussian dispersal kernel [Eq. (A.6)]. Solid curve shows the R_0 computed by solving the eigenvalue problem in Eq. (A.3). Dotted curves represent the approximate $R_{0c}(x_0, y_0)$, according to Eq. (A.5) with the initial inoculum located at the field center ($x_0 = y_0 = d/2$, upper curve), at the field border ($x_0 = d/2, y_0 = 0$, middle curve) and in the corner of the field ($x_0 = 0, y_0 = 0$, lower curve). The dashed curve shows the average $\langle R_{0c}(x_0, y_0) \rangle_{x_0, y_0}$ over the field, according to Eq. (A.8). Model parameters: $\beta = 4$, $K = 1$, $\mu = 2$.

A.3. Estimation of the basic reproductive number as a function of the field size and shape

The basic reproductive number, R_0 can be determined as the dominant eigenvalue of the Fredholm equation Eq. (A.3) We compute it as a function of the dimensions d_x and d_y of a rectangular field, which characterize its size and shape. To do this, we obtain numerical estimates for the dispersal kernel $\kappa(r)$ (Sec. A.3.1 and Sec. A.3.2) and the parameter combination $\beta K/\mu$ (Sec. A.3.3), which as we will show corresponds to the limit of R_0 at $d_x, d_y \rightarrow \infty$.

A.3.1. Fitting disease gradients

Disease gradients were measured in terms of both average number of lesions per leaf and disease severity in a large-scale experiment over three consecutive seasons (Sackett and Mundt, 2005a; Cowger et al., 2005). The datasets corresponding to the average numbers of lesions per leaf in primary disease gradients were fitted using several different model functions (Sackett and Mundt, 2005a). Here, we also fitted the disease severity measurements corresponding to primary disease gradients (Fig. A.2) for the two largest datasets (Hermiston 2002 and Madras 2002) of the experiments (Sackett and Mundt, 2005a; Cowger et al., 2005).

The following model functions are often used to fit the disease gradient data. Lambert kernel (Lambert et al., 1980)

$$y_L(r) = y_0 \exp[-(r/a)^n], \quad (\text{A.11})$$

which includes the special cases of the exponential (or Laplacian) kernel at $n = 1$ and the Gaussian kernel at $n = 2$. Power-law kernel (Gregory, 1968)

$$y_{PL}(r) = y_0 r^{-b} \quad (\text{A.12})$$

is used to describe disease gradients of pathogens with long-range dispersal. However, the function approaches infinity at the focus $r = 0$, which is unrealistic. For this reason a modified power-law kernel was introduced (Mundt and Leonard, 1985)

$$y_{PL1}(r) = y_0 (r_0 + r)^{-b}. \quad (\text{A.13})$$

It exhibits the same behavior as the power-law kernel in Eq. (A.12) at large r , but the divergence is “softened” such that the function has a finite value at $r = 0$. In this study, we used a different form of the modified power-law kernel

$$y_{PL2}(r) = y_0 (r_0^2 + r^2)^{-b/2} \quad (\text{A.14})$$

that is very similar to Eq. (A.13), but is more suitable for extensive numerical computations required for the solution of the eigenvalue problem in Eq. (4).

Figure A.2 shows the primary disease gradients in terms of the disease severity for the two largest datasets obtained in (Cowger et al., 2005; Sackett and Mundt, 2005a): Hermiston 2002 (left panel) and Madras 2002 (right panel). Both of the datasets were fitted using the exponential kernel [Eq. (A.11) with $n = 1$], Lambert kernel [Eq. (A.11)], modified power law 1 [Eq. (A.13)] and modified power law 2 [Eq. (A.14)]. The two modified power laws provided best fits with the

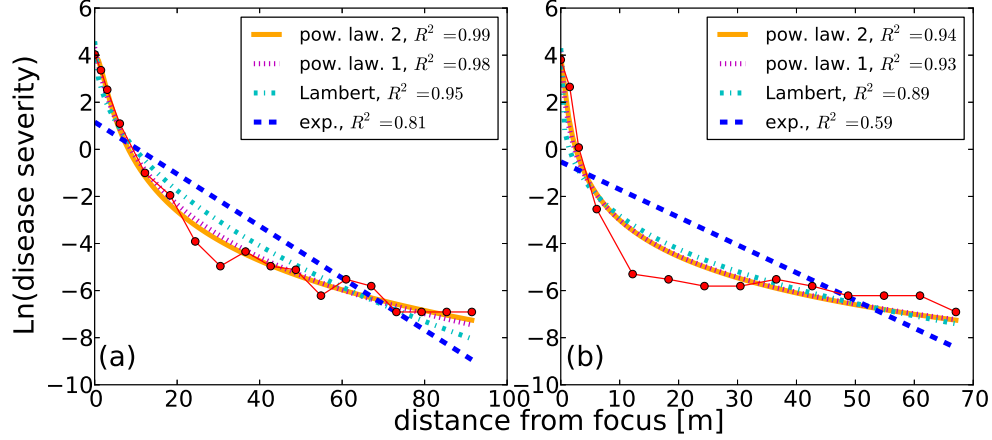


Figure A.2: Disease gradient data (circles) from Hermiston 2002 downwind [left panel (a)] and Madras 2002 downwind [right panel (b)] experiments conducted by Sackett and Mundt (2005a); Cowger et al. (2005). Natural logarithm of disease severity is shown versus the distance from focus. The data was fitted by four functions: exponential [Eq. (A.11) with $n = 1$], Lambert [Eq. (A.11)], modified power law 1 [Eq. (A.13)] and modified power law 2 [Eq. (A.14)].

modified power law 2 being slightly better. It is our kernel of choice, since it also allows for faster numerical solutions of the eigenvalue problem in Eq. (4).

The fit of the modified power-law function in Eq. (A.14) to the disease gradient data shown in Fig. A.2 yielded the following estimates for the parameter values:

$$\text{Hermiston 2002 downwind } r_0 = 2.2255 \text{ m}, b = 3.0365, y_0 = 6.4424; \quad (\text{A.15})$$

$$\text{Madras 2002 downwind } r_0 = 0.4486 \text{ m}, b = 2.2345, y_0 = 0.085127. \quad (\text{A.16})$$

A.3.2. Definition and normalization of the dispersal kernel

We defined the dispersal kernel $\kappa(x, y, u, v)$ as a probability density function for an infectious spore to land at a distance r from its source (Nathan et al., 2012). A spore should eventually land somewhere is reflected in the condition to normalize the dispersal kernel:

$$\int_0^{2\pi} d\theta \int_0^\infty dr r \kappa(r, \theta) = 1. \quad (\text{A.17})$$

Here, we transformed the dispersal kernel to polar coordinates using the relationships $x = r \cos \theta$, $y = r \sin \theta$. In the case of isotropic dispersal $\kappa(r, \theta) = \kappa(r)$, i. e. the dispersal kernel does not depend on the angle of dispersal θ . Then the normalization condition reads

$$2\pi \int_0^\infty dr r \kappa(r) = 1. \quad (\text{A.18})$$

Next, we provide the normalization condition for the modified power-law function $Y_{\text{PL2}}(r)$ [Eq. (A.14)] and for the Lambert function [Eq. (A.11)].

The dispersal kernel $\kappa(r)$ is assumed to be proportional to the disease gradient $y(r)$ (see Sec. 3.2). Therefore, the dispersal kernel should be given by the same function as the disease gradient

$$\kappa_{\text{PL2}}(r) = \kappa_{0\text{PL2}} (r_0^2 + r^2)^{-b/2}, \quad (\text{A.19})$$

but with the different proportionality constant κ_0 , which is obtained by substituting the Eq. (A.19) into the normalization condition Eq. (A.18):

$$\kappa_{0\text{PL2}} = (b - 2)r_0^{b-2}/(2\pi). \quad (\text{A.20})$$

This expression is valid only if the integral in Eq. (A.18) converges, which is the case at $b > 2$. In both datasets used here (Hermiston 2002 and Madras 2002 downwind) this condition is fulfilled for the values of b , corresponding to the best fit.

Similarly, the Lambert dispersal kernel has the form:

$$\kappa_{\text{L}}(r) = \kappa_{0\text{L}} \exp[-(r/a)^n], \quad (\text{A.21})$$

where

$$\kappa_{0\text{L}} = \frac{1}{\pi a^2 \Gamma\left(\frac{2+n}{n}\right)} \quad (\text{A.22})$$

is determined from the normalization condition Eq. (A.18).

We use the numerical values for the best-fit parameters Eq. (A.15) and Eq. (A.16) to obtain estimates for κ_0 using Eq. (A.20):

$$\text{Hermiston 2002 downwind : } \kappa_0 = 0.3780, \quad (\text{A.23})$$

$$\text{Madras 2002 downwind : } \kappa_0 = 0.03092. \quad (\text{A.24})$$

Thus, our estimates for the dispersal kernels $\kappa(r)$ are given by the Eq. (A.19) with the parameter values from Eq. (A.15) and Eq. (A.23) for Hermiston 2002 downwind; and from Eq. (A.16) and Eq. (A.24).

A.3.3. Estimation of the R_0 in the limit of a large field size

First, we consider the host population to be initially fully susceptible and have the leaf area index of K_0 . Then, we introduce a localized unit of infected hosts (focus) at a position x_0, y_0

$$H(x, y, t = 0) = K, \quad I(x, y, t = 0) = I_{\text{tot0}} \delta(x - x_0) \delta(y - y_0). \quad (\text{A.25})$$

We are interested here only in the primary infections occurring due $I(x, y, t = 0)$, because the amount of disease due to the primary infection (or the primary disease gradient) is often measured in experiment (for example, (Sackett and Mundt, 2005a)). Hence, we derive the amount of

infection produced after a single time step Δt from Eq. (2):

$$[I(x, y, t = \Delta t) - I(x, y, t = 0)] / \Delta t = \quad (\text{A.26})$$

$$\beta \int_0^{d_x} du \int_0^{d_y} dv \kappa(x, y, u, v) I(u, v, t = 0) H(x, y, t = 0) - \mu I(x, y, t = 0) \quad (\text{A.27})$$

By substituting Eq. (A.25) in Eq. (A.26) we obtain

$$\Delta I(x, y, t = \Delta t) = I_{\text{tot}0} \Delta t K_{\Delta t} \beta \kappa(x, y, x_0, y_0), \quad (\text{A.28})$$

where

$$\Delta I(x, y, t = \Delta t) = I(x, y, t = \Delta t) - I(x, y, t = 0) \quad (\text{A.29})$$

represents the primary disease gradient from a localized point-like source. Further, we assume dispersal to be isotropic and set the coordinate of the focus to zero, i.e. $x_0 = 0$. Then, the amount of infected host in the next time step and the dispersal function depend only on the distance $r = \sqrt{x^2 + y^2}$ from the focus, i.e. $I(x, y, t = \Delta t) = I(r, t = \Delta t)$, $\kappa(x, y, x_0, y_0) = \kappa(r)$. We can then re-write the Eq. (A.28):

$$\Delta I(r, t = \Delta t) = I_{\text{tot}0} \Delta t K_{\Delta t} \beta \kappa(r), \quad (\text{A.30})$$

Next, we connect $\Delta I(x, y, t = \Delta t)$ with the whole-plant disease severity $y(r)$.

The quantity $I(r, t)$ in our model that represents the spatial density of the infected host tissue. In the case of wheat stripe rust it is the infected leaf area per unit land area (in analogy with the ‘‘leaf area index’’ (LAI), we will call it the ‘‘infected leaf area index’’ (ILAI)). We express the disease severity as a ratio $y(r) = \mathcal{I}(r) / \mathcal{K}_{\Delta t}$, where $\mathcal{I}(r)$ is the total infected leaf area at a location r and $\mathcal{K}_{\Delta t}$ is the total leaf area at a location. By dividing both the numerator and the denominator of this expression by the unit land area Δs , we obtain $y(r) = \Delta I(r) / K_{\Delta t}$, where $\Delta I(r)$ is given by Eq. (A.29), and $K_{\Delta t}$ is the total leaf area index. Therefore,

$$\Delta I(r, t = \Delta t) = K_{\Delta t} y(r). \quad (\text{A.31})$$

On the other hand, from Eq. (A.30)

$$\Delta I(r, t = \Delta t) = \beta K_{\Delta t} \Delta t I_{\text{tot}0} \kappa(r). \quad (\text{A.32})$$

By equating Eq. (A.31) and Eq. (A.32) we obtain the relationship

$$\frac{\beta}{\mu} = \frac{1}{I_{\text{tot}0}} \frac{y(r)}{\kappa(r)}. \quad (\text{A.33})$$

Here we assumed $\Delta t = 1/\mu$, which implies that the consecutive pathogen generations do not overlap (see the discussion in Sec. A.1). We multiply both sides of the Eq. (A.33) by the leaf area index $K_{\Delta t}$ at time $t = \Delta t$ and obtain the expression for $R_{0\infty} = \beta K_{\Delta t} / \mu$

$$R_{0\infty} = \frac{K_{\Delta t} Y_0}{I_{\text{tot}0} \kappa_0}. \quad (\text{A.34})$$

Here we used the fact that $\kappa(r)$ is proportional to $Y(r)$ and, therefore, their ratio equals to the ratio Y_0/κ_0 .

Now, we determine the intensity of the initial inoculum $I_{\text{tot}0}$ [Eq. (A.25)] from experimental parameters. The δ -functions in Eq. (A.25) represent an infinitely narrow peak of a unit height. This is an idealized mathematical entity that can, however, be quite useful. It describes the actual situation well if the spatial scale of interest is much larger than the size of the focus. This was the case in the studies (Sackett and Mundt, 2005a; Cowger et al., 2005), where the focus (the area inoculated initially) was a square with the side $\Delta x_f = 1.52$ m, while the spatial scale over which the epidemic developed in the next generation was 50-80 m for the two largest datasets (Hermiston 2002 and Madras 2002 downwind).

$$\int_0^{\Delta x_f} dx \int_0^{\Delta x_f} dy I_{\text{tot}0} \delta(x - x_0) \delta(y - y_0) = I_{\text{tot}0} = \int_0^{\Delta x_f} dx \int_0^{\Delta x_f} dy I_0 = y_0 K_0 \Delta x_f^2. \quad (\text{A.35})$$

Here, y_0 is the disease severity at the focus caused by artificially inoculated spores (first generation) and K_0 is the leaf area index at the time of inoculation (“zeroth” generation). The Eq. (A.35) says what the intensity of the initial inoculum should be if it was concentrated in a very small area such that the total amount of disease is the same as in the experiment.

$$I_{\text{tot}0} = y_0 K_0 \Delta x_f^2. \quad (\text{A.36})$$

After substituting Eq. (A.36) into Eq. (A.34) we obtain:

$$R_{0\infty} = \frac{K_{\Delta t}}{K_0} \frac{1}{y_0 \Delta x_f^2} \frac{Y_0}{\kappa_0}. \quad (\text{A.37})$$

The expression in Eq. (A.37) now consists of the parameters that are known from a typical disease gradient experiment.

We use the estimates we obtained above for the parameters Y_0 [Eq. (A.15) and Eq. (A.16)] and κ_0 [Eq. (A.23) and Eq. (A.24)], also use the area of the focus $\Delta x_f^2 = 1.52 \text{ m} \times 1.52 \text{ m} = 2.31 \text{ m}^2$ for both datasets and the values for the initial disease severity $y_0 = 0.227$ (Hermiston 2002) and $y_0 = 0.062$ (Madras 2002) (Cowger et al., 2005). We also assume that the leaf area index at the time of inoculation K_0 was two times smaller than its value at the time of disease gradient measurement, when the plants almost reached their maximum size, i. e. $K_{\Delta t} = 2K_0$. By substituting these values into Eq. (A.37) we obtain the estimates for $R_{0\infty}$:

$$\text{Hermiston 2002 downwind } R_{0\infty} = 65.0; \quad (\text{A.38})$$

$$\text{Madras 2002 downwind } R_{0\infty} = 38.0. \quad (\text{A.39})$$

Having obtained the numerical values for the parameter $R_{0\infty} = \beta K_{\Delta t} / \mu$ and the function $\kappa(r)$, we solved the eigenvalue problem in Eq. (A.3) numerically for different values of d_x and d_y and determined the basic reproductive number R_0 as a function of the field size and shape. The results of this computation are shown in Fig. 3 and Fig. 4.

A.4. Susceptible-infected model with spatial spore dispersal

In this section we consider the model that takes into account spore dynamics explicitly. Our goal here is to describe the approximation that was used to obtain the simplified model Eqs. (1)-(2) that do not explicitly include spore dynamics. For the sake of brevity we consider the model in one-dimensional space, but it is straightforward to extend the consideration to two dimensions. The model of host-pathogen population dynamics reads

$$\frac{\partial H(x, t)}{\partial t} = r_H(K - H(x, t)) - \beta' \int_0^d \kappa(|s - x|)U(s, t)ds H(x, t), \quad (\text{A.40})$$

$$\frac{\partial I(x, t)}{\partial t} = \beta' \int_0^d \kappa(|s - x|)U(s, t)ds H(x, t) - \mu I(x, t), \quad (\text{A.41})$$

$$\frac{\partial U(x, t)}{\partial t} = \gamma I(x, t) - \mu' U(x, t), \quad (\text{A.42})$$

where $H(x, t)$, $I(x, t)$ represent the areas covered by susceptible and infected host tissue, correspondingly, per unit area of the field; and $U(x, t)$ represents the number of spores per unit area of the field. Susceptible hosts $H(x, t)$ grow with the rate r_H . Their growth is limited by the ‘‘carrying capacity’’ K , implying limited space or nutrients. Furthermore, susceptible hosts $H(x, t)$ may be infected by the pathogen and transformed into infected hosts in the compartment $I(x, t)$ with the transmission rate β' . The corresponding terms in Eqs. (A.40)-(A.41) are proportional to the amount of the available susceptible tissue $H(x, t)$ and to the amount of the infectious spores $U(x, t)$ at the location x . Infectious spores are produced at the rate γ and lost at the rate μ' .

Here, $\kappa(|s - x|)$ is the dispersal kernel that characterizes the probability of an infectious spore, produced at the location s to land at the location x . The integration is performed over all possible sources of spores within the field, i. e. over the whole extension of the field from 0 to d , where d is the size of the field. We assume that the dispersal kernel depends only on the distance $|s - x|$. The fact that the spore should land somewhere allows to normalize this function such that the integral of it over the whole space is unity:

$$\int_0^\infty \kappa(r)J(r)dr = 1, \quad (\text{A.43})$$

where $J(r) = 1$ for the one-dimensional case considered here, and $J(r) = r$ for the two-dimensional case (in this case additional integration over the polar angle is required).

We assume that the characteristic time scale of spore dispersal is much shorter than the characteristic time scales associated with other stages of the pathogen life cycle. Then, the equation for spores is assumed to quickly assume the equilibrium state, with the left-hand side equal to zero and $U(x, t) = (\gamma/\mu')I(x, t)$. This means that the density of spores is proportional the density of the infectious host tissue. By substituting this expression into Eqs. (A.40)-(A.42), we reduce the model to just two Eqs. (1)-(2), where the transmission rate is a compound parameter: $\beta = \gamma\beta'/\mu'$.

A.5. The relationship between the basic reproductive number and the epidemic velocity

For the susceptible-infected epidemiological model where the transmission of disease through space is described using the diffusion term (proportional to the Laplacian of $I(x, y, t)$), the wave speed of the epidemic, c , is proportional to $\sqrt{R_0 - 1}$ (Keeling and Rohani, 2008). This relationship holds in the case of very local dispersal: the diffusion term can be obtained from a more general formulation in terms of a system of integro-differential equations by performing the Taylor series expansions under the assumption that the dispersal is sufficiently local. In addition, this requires that the average dispersal distance is finite, and hence the dispersal kernel must decay faster than r^{-3} .

In our case the dispersal is nonlocal and is governed by empirically determined dispersal kernels that exhibit power-law behavior. In this case, it is not straightforward to determine the analytical relationship between the basic reproductive number and the epidemic velocity. A numerical investigation can be performed by solving the system of Eqs. (1)-(2) numerically with the parameters corresponding to different values of R_0 and determining the epidemic velocity.

However, we can still use the relationship $c \propto \sqrt{R_0 - 1}$ as a rough lower estimate for the epidemic velocity in this case. Then, the ratio between the epidemic velocities c_1 and c_2 in plots with different sizes and geometries reads:

$$\frac{c_1}{c_2} = \sqrt{\frac{R_{01} - 1}{R_{02} - 1}}, \quad (\text{A.44})$$

where R_{01} and R_{02} are the basic reproductive numbers in these two different plots. We obtained the following estimates for the basic reproductive numbers that correspond to the two plot sizes and geometries (plot 1: 61 m \times 61 m; plot 2: 6.1 m \times 61 m) used in the experiments (Sackett and Mundt, 2009) (these are marked as white and gray circles in Fig. 4)

$$\text{Hermiston 2002} : R_{01} = 57.75, R_{02} = 34.91; \quad (\text{A.45})$$

$$\text{Madras 2002} : R_{01} = 22.83, R_{02} = 15.41; \quad (\text{A.46})$$

Substituting these values in Eq. (A.44) leads to the following approximate ratios of the epidemic velocities:

$$\text{Hermiston 2002} : \frac{c_1}{c_2} = 1.286; \quad (\text{A.47})$$

$$\text{Madras 2002} : \frac{c_1}{c_2} = 1.217. \quad (\text{A.48})$$

Thus, we predict a moderate difference in epidemic velocities in these two plots, while the empirical study (Sackett and Mundt, 2009) reported no detectable difference. We suggest two possible explanations for this discrepancy. First, our model assumed isotropic dispersal and neglected the influence of the prevailing wind direction, while in the experimental setting of (Sackett and Mundt, 2009), there was a strong anisotropy in dispersal due to wind. Strongly directional wind may be capable of masking the effect of plot size and geometry on R_0 and epidemic velocity. This is because the smaller or narrower plots decrease pathogen fitness due to the edge effect, i. e. due to the

pathogen spores that were lost outside the plot. In the presence of a strong wind, in an elongated plot, the spores that would have been lost outside the plot may well remain inside and contribute to the development of the epidemic. This effect is expected to be strongest when the prevailing wind direction coincides with the longer axis of the plot, as was the case in the experimental setting (Sackett and Mundt, 2009). On the contrary, we expect the effect of the plot size and geometry to be magnified by wind, when the wind direction is perpendicular to the longer axis of the plot. A second possible factor that may contribute to the discrepancy is the experimental resolution: it may be challenging to be able to detect differences in epidemic velocities of 20-30 % that we predict in (A.47), (A.48).